Growth Cone Dynamics and Vesicle Trafficking in Developing Neurons In Vitro

Broeke, J.H.P.

2011

document version
Publisher's PDF, also known as Version of record

APPENDIX A

MATHEMATICAL FRAMEWORK FOR A RECURSIVE BAYESIAN ESTIMATION ALGORITHM

1. INTRODUCTION

Tracking objects such as vesicles requires two important steps: detection and tracking. Detection requires that objects can be isolated from the background. Furthermore, it is also necessary to describe different objects in such a way that they later can be uniquely identified. The tracking step involves linking of detected objects and linking them over time into a track. This appendix will describe an algorithm that uses Bayesian statistics to link the detected objects and create tracks of unique objects over time.

2. DETECTION

Detection of vesicles involves the identification and isolation of the image into regions that correspond to objects of interest. Figure 1A shows zoomed part of a microscopy image containing vesicles from a time lapse series. Imaged using standard epi–fluorescence, this image possesses some characteristics that are common to fluorescent neuronal culture images: high noise level and image artifacts, non–uniform background, variant brightness of vesicles introduced by inherent heterogeneity of the staining, variability of vesicle shapes and sizes, and partial occlusion and clustering of vesicles. These characteristics render difficulty in detecting vesicles. On the other hand, however, there are some characteristics also available for use. Assume the image series has dimensions $X \times Y$ pixels, K frames long, corresponding to each element (x, y, k), for $x = 1, \dots, X$, $y = 1, \dots, Y$ and $k = 1, \dots, K$, in the series there is an intensity or gray level value $i(x, y, k)$. We create a maximum intensity projection map (Figure 1B) by projecting intensity values along the K (time) axis, that is, for each pixel of the map, its intensity is obtained by

$$i(x, y) = \max_k \big(i(x, y, k)\big) \tag{1}$$

We discover from the map that the movement of vesicles is confined to certain tracks (shown as the bright regions). Figure 1C depicts the histogram of the projection map. The histogram is jagged but can be seen to consist of two modes. The left mode is predominant, corresponding to background. The right one is isolated and formed by vesicles with high brightness. The long, flat and low valley between the two modes is a joint contribution of uneven background and widely spread vesicle intensity. This suggests a threshold can be chosen within the valley to roughly identify the region that contains the vesicles. We adopt a range method (Sezgin and Sankur, 2004) since the image is dominated by the background and therefore, the range of the background can be approximated by the mean and standard deviation of the pixels in the image. A pixel is classified as a vesicle pixel if its intensity is not in the background range:

$$i(x, y) > \mu + \alpha \cdot \sigma_1 \tag{2}$$

where α controls the bias, a lower α value would include more background pixels, while a higher α is more risky to miss out vesicles. Figure 1D shows the initial

segmentation of Figure 1A with α set to 1.2. It is possible to use other thresholding techniques, e.g. the Otsu' intermeans method (Otsu, 1979) found also performing well in some of our test images.

The identified pixels need a further screening. Each pixel is examined based on its local spatial and intensity information. Define the local area of the pixel as a $W \times W$ window centered at that pixel (Figure 2A); first calculate the local intensity histogram (Figure 2C). The histogram is often very jagged with separated local minima and maxima; at first glance it does not provide clear information. We propose to smooth the histogram by convolving it with a 1D Gaussian window (note that other smoothing methods, e.g. n point moving average, may be used), the improved histogram (Figure 2D) clearly reveals the constituted modes. The first meaningful minimum T to the right of the biggest peak is chosen as the refined threshold, if the pixel intensity $i(x, y) < T$, it will be discarded as a background pixel.

While in most situation a pixel with intensity value higher than T is a vesicle pixel, there are cases where it may be misclassified. For example, a pixel located between two

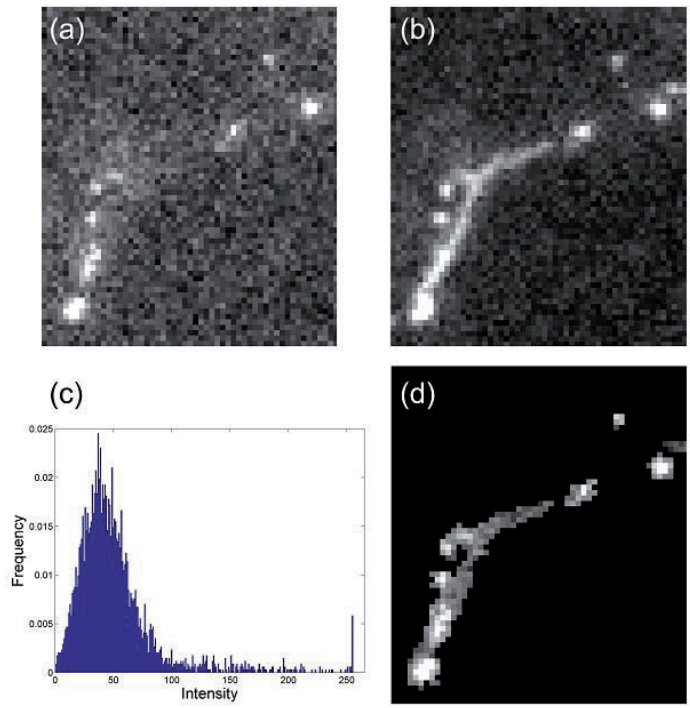

Figure 1: Segmentation of the vesicle paths. Obtaining the approximate region that contains the vesicles. (a) A frame of the image sequence. (b) Map of the maximum intensity projection along the time axis, in which vesicle region has a better contrast to the noisy background. (c) The histogram of the projection map in (b). (d) A global threshold is applied to segment the image in (a), which removes most of the background.

closely spaced vesicles may have higher intensity. We propose to examine the local spatial configuration of the pixel before assignment in these difficult cases. The step is illustrated in Figure 2B. The local $W \times W$ window is divided into a central block B_0 and 8 neighbor blocks $B_1, \ldots, B_8$. In the illustration, $w = 9$ and each block contains 3×3 pixels. Compare the mean intensity of the central block with its neighbors, defining

$$c\left(\mu_{B_0}, \mu_{B_j}\right) = \begin{cases} 1 & \text{if } \mu_{B_0} > \alpha \cdot \mu_{B_j} \\ 0 & \text{if } \mu_{B_0} \leq \alpha \cdot \mu_{B_j} \end{cases} \tag{3}$$

where $j = 1, \ldots, 8$ and μ_{B_0} is mean block intensity, bias $\alpha > 0$ controls the contrast. Count the number of neighbor blocks that has lower mean than the central block, $n(B) = \sum_{j=1}^{8} c\left(\mu_{B_0}, \mu_{B_j}\right)$, $n(B)$ is an indication of probability that the center pixel

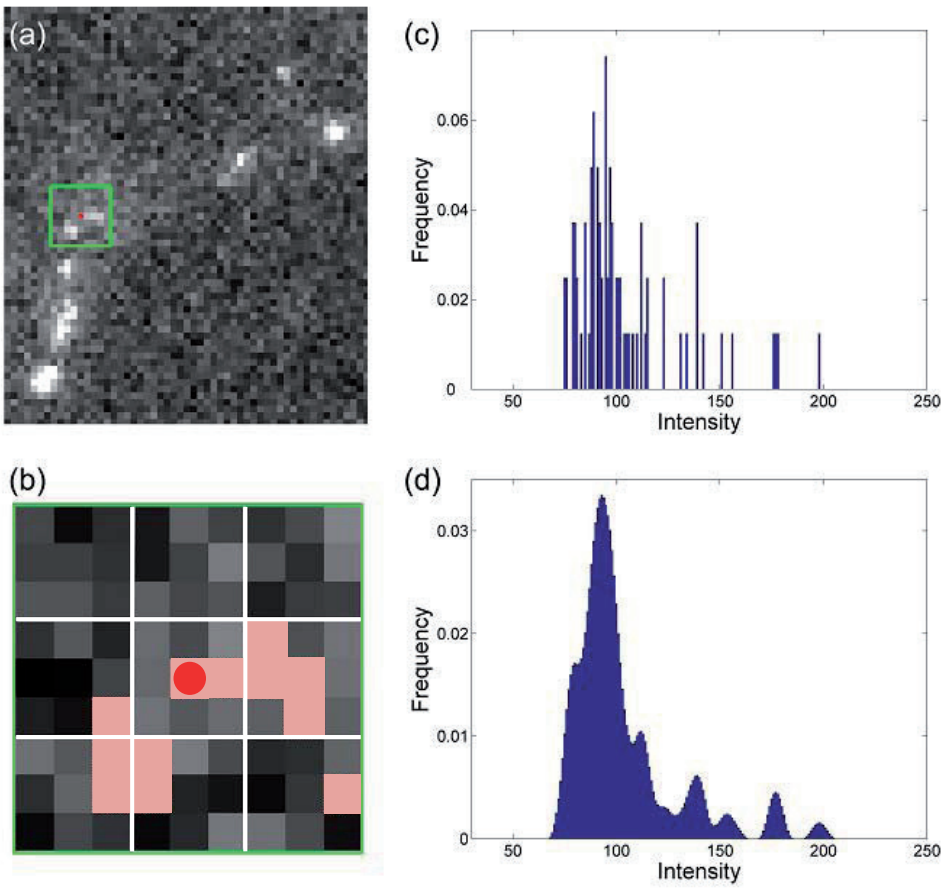

Figure 2: Local analysis. Illustration of local analysis. (a) The pixel (red) has a 9 × 9 local area defined. (b) Local spatial configuration. (c) The intensity histogram of the local intensity. (d) The smoothed histogram in (c).

(x, y) belongs to a vesicle. In experiment we use a hard rule that a pixel is classified as vesicle pixel if $n(B)$ is greater than a threshold value of 5. To minimize the influence of background, only window pixels with intensity higher than T (marked with red texture) are included in the blocks.

3. TRACKING

An essential requirement for tracking a vesicle is to determine its position in each frame of the image sequence. When the number of vesicles is fixed, given the previous detection step producing a perfect result, that is, no vesicle is missed (unity probability of detection) and all detected objects are true vesicles (zero false alarm rate), this task is reduced to link objects between the frames. A simple and commonly used approach to linking is nearest neighbor association (NNA (Ku et al., 2007)). For an object in the current frame, its distance measure to all other objects in the next frame is computed, and the object pair with the shortest distance is linked as the same vesicle. The NNA assumes the small displacement of the objects, tracking based on this approach is deterministic.

As the dynamics of the objects deviate from its assumptions, the performance of NNA tracking deteriorates quickly. Actually, in our problem these assumptions no longer hold. Furthermore, the varying number of vesicles across frames and the possibility of missed detection in the presence of false alarms (clutters) cause additional uncertainty in tracking. A successful tracking algorithm must address these uncertainties and we propose a probabilistic treatment.

3.1 Modeling objects

Since tracking of objects is the process of determining their kinematic characteristics, an individual object can be represented using a state vector. In our method, this state is defined as:

$$\mathbf{x}_{k,i} = \{x_{k,i}, \dot{x}_{k,i}, A_i\} \tag{4}$$

where the subscript k, i indicates that it is the ith object's state in image frame k, $x_{k,i}$ specifies the location and $\dot{x}_{k,i}$ the motion, A_i is the appearance model of the object. We have shown that the lack of regular pattern in the appearance of objects makes it difficult to formulate a general model for detection, which implies that a specific model for individual object can be established to aid tracking. We choose to represent the object in terms of its internal characteristics (the pixels comprising the object (Gonzalez et al., 2002)) and the feature selected as descriptor is gray-level intensity.

Normally, the appearance model is generated and fixed when the object is initially identified. For example, the object $\mathbf{x}_i$ is selected for tracking from the first frame and its

track lasts for six frames, then its appearance model is generated in the first frame based on its location $x_{1,i}$. In the case of changing illumination and/or other imaging conditions having caused significant change of object appearance between frames, an adapted object model can be adopted.

In generation of the appearance model (Figure 3) for object $\mathbf{x}_i$, the smallest rectangle containing its region is first determined. This can be done either manually, or as in our experiments, automatically by a detection module (Section 1). Within this rectangle, the pixel intensity distribution A_i is calculated using m-bin histogram discretization (Comaniciu et al., 2000) $A_i = \{p_u(x_{1,i})\}_{u=1\ldots m}$, is a kernel estimate of the probability of occurrence of intensity level u:

$$p_u(x_{1,i}) = C \sum_s K\left(\frac{x_{1,i} - \mathbf{s}}{\mathbf{d}}\right) \delta(\mathbf{b}(\mathbf{s}) - u) \tag{5}$$

where each pixel in the rectangle has relative location $\mathbf{s}$ in relation to the centroid $x_{1,i}$. $\mathbf{d} = [d_x, d_y]^T$ specifies the half width of the rectangle along each dimension and is used to scale the size to the unit length. C is the normalization constant to ensure $\sum_{u=1}^{m} p_u(x_{1,i}) = 1$. A pixel is assigned to the corresponding bin by the function $\mathbf{b}(\mathbf{s})$ according to its intensity value, δ is the Kronecker delta function. The kernel K associates a weight to each pixel. A smooth kernel such as Epanechnikov kernel (Cheng, 1995) can be used:

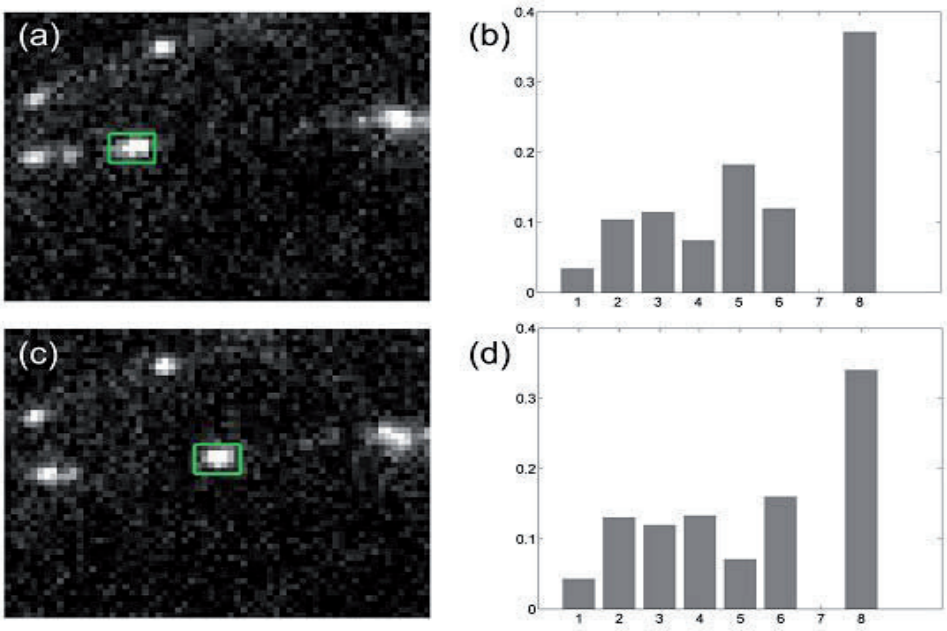

Figure 3: The appearance model. An example of the appearance model used for tracking. At frame 1 the appearance model (b) is generated for a target vesicle (a). During the tracking process, this model will be compared to the appearance (d) of the measured vesicle candidate (c).

$$K(r) = \begin{cases} 1 - \|r\|^2 & \text{if } \|r\| \leq 1 \\ 0 & \text{if } \|r\| > 1 \end{cases} \quad (6)$$

by assigning smaller weights to pixels farther from the object centroid, it increases the reliability of distribution estimates since the boundary pixels are often believed to be affected by occlusions or background (Comaniciu et al., 2003). But, when a object has a very small size, we suggest a flat kernel to avoid participating pixels in the estimation too few:

$$K(r) = \begin{cases} 1 & \text{if } \|r\| \leq 1 \\ 0 & \text{if } \|r\| > 1 \end{cases} \quad (7)$$

3.2 A framework for optimal tracking

As an example, Figure 4 shows the complications of object tracking. During the process, the following events may occur:

- » Update: an existing object is evolved from one frame to the next
- » Birth: a new object is added.
- » Death: an existing object disappears in the next frame.
- » Merge: several existing objects are merged into a single object in the next frame.
- » Split: an existing object is divided into several objects in the next frame.

Therefore by state representation of an object as in Eq. (4), the established object tracks in each frame k is a finite random set $X_k = \{\mathbf{x}_{k,1}, \dots, \mathbf{x}_{k,n(k)}\}$ where $n(k)$ is the varying number of objects and $\mathbf{x}_{k,i}, i = 1, \dots, n(k)$ are individual object states. The evolution of the set is characterized by the motion model

$$X_k = S_k(X_{k-1}) \cup \Gamma_k(X_{k-1}) \cup \Psi_k(X_{k-1}) \cup B_k \quad (8)$$

which states that the set X_k of object tracks in current frame k consists of the set S_k of tracks updated from the previous frame $k-1$, the sets Γ_k and Ψ_k of new objects that are formed by merge and split of (part of) objects X_{k-1} in previous frame $k-1$, and the set B_k of new objects which appear spontaneously in frame k.

As shown in Figure 4, due to limitation of the imaging and detection, measured objects may include false alarms or clutters. In addition, some objects may have their measurements overlapped (data not shown), while some others may not be detected. As a result, the set of measurements $I_k = \{\mathbf{z}_{k,1}, \dots, \mathbf{z}_{k,m(k)}\}$ is also random, where $m(k)$ is the number of measurements and $\mathbf{z}_{k,i}, i = 1, \dots, m(k)$ is the single object measurement state $\mathbf{z}_{k,1} = \{z_{k,i}, A^*_{k,i}\}$ in which z_{k-1} gives the detected object location and $A^*_{k,i}$ the associated appearance computed using Eq. (5).

The presence of uncertainty prompts a probabilistic tracking. Using to denote the object tracks over the sequence of images, to denote the corresponding measurements, tracking can be formulated as computing the posterior density $p(X_{1:K}|I_{1:K})$ that fits naturally into a Bayesian recursion (Mahler, 2003), for $2 \leq k \leq K$,

$$p(X_k|I_{1:k-1}) = \int p(X_k|X_{k-1})p(X_{k-1}|I_{1:k-1})\delta X_{k-1} \quad (9)$$

$$p(X_k|I_{1:k}) \propto p(I_k|X_k)p(X_k|I_{1:k-1}) \quad (10)$$

where $\int \cdot \delta X$ is the set integral, $p(X_k|X_{k-1})$ is the transition density. The density form of the motion model (Eq. (8)), which incorporates our knowledge about the internal dynamics of the objects and predicts the object tracks at current frame k given the previous track set X_{k-1}. $p(I_k|X_k)$ is the density form of the measurement model, which serves as the likelihood function and expresses the probability we would have measured objects I_k given the track set X_k in frame k.

The recursive equations (9) and (10) provide a theoretically rigorous approach to optimally track a variable number of objects over an image sequence. However, computation of the joint posterior density $p(X_k|I_{1:k})$ over object states is in general an intractable problem, for it requires solving a combinatorial sum of integrals of high dimensions with a prohibitively large number of combinations even for medium number of targets. There are some methods that have been proposed to ease the computational complexity. One class of methods is based on the probability hypothesis density (PHD (Mahler, 2002; Vo et al., 2005)), the first moment of joint distribution whose integral over any sub-area in state space is the expected number of objects in that area. The PHD method brings the recursion into a computationally feasible form by propagating the first moment in the place of the posterior distribution itself. In general, this method does not maintain the identities of objects[†], while our tracking problem requires the temporal association of estimated object states over time so that individual object track can be established. Another class of methods relies on the disassembly of the joint state estimation into a collection of conditional independent single object tracking. The representative methods of this kind include the multiple hypothesis tracking (MHT (Reid, 1979)), the joint probabilistic data association (JPDA (Shalom and Fortmann, 1988)) and their variations (Blackman and Popoli, 1999). The core of these methods is to form the most likely model-data association. Our implementation of the object tracking is based on the idea of MHT.

3.3 Multiple hypothesis tracking (MHT)

In our representation of the set of objects in each frame (Figure. 4) by X_k, $k = 1, \dots, K$, it is implicitly assumed that the state $\mathbf{x}_{k,i}$ of each object has a unique identifier $\tau_{k,i}$ attached to it, i.e., $(\mathbf{x}_{k,i}, \tau_{k,i})$. $\tau_{k,i}$ is called the object track ID. Suppose there are in total N_K objects in the sequence of K images, each object track is assigned a unique ID ranging from 1 to N_K, then $\tau_{k,i} \in \{1, \dots, N_K\}$. Writing explicitly, for each set X_K, there is a corresponding object ID set $\mathcal{T}_k$. Likewise, each measurement set I_k has an associated index set $\mathcal{M}_k$, which is the subset of $\{1, \dots, M_k\}$ where M_k is the total number of

[†] For linear Gaussian multi-target models, a closed-form solution to the PHD recursion may be derived to include object identity (Clark et al., 2006).

measurements. For each frame, we introduce an association hypothesis h_k as a relation on the set $(\{0\} \cup \mathcal{T}_{k-1}) \times (\{0\} \cup \mathcal{M}_k)$:

$$h_k = \{(n, m) | n \in \{0\} \cup \mathcal{T}_{k-1}, m \in \{0\} \cup \mathcal{M}_k\} \tag{11}$$

The h_k links the existing object tracks to newly received measurements. By $h_k(n, m)$, $n \neq 0$ and $m \neq 0$, it means that measurement m is associated to object n. By $h_k(n, 0)$, $n \neq 0$, it means that object track n is not detected and generates no measurement, and by $h_k(0, m)$, $m \neq 0$, it means that measurement m is not associated with any object track. With the introduction of h_k, the representation of set of objects in frame k is augmented from X_k to (X_k, h_k). Correspondingly, the Markov transition density $p(X_k|X_{k-1})$ that characterizes the dynamics of the object set becomes $p(X_k, h_k|X_{k-1}, h_{k-1})$; the likelihood function $p(I_k|X_k)$ characterizing the measurement process becomes $p(I_k|X_k, h_k)$. Tracking of objects over the image sequence can therefore be formulated as to estimate $p(X_k, h_k|I_{1:k})$ recursively:

$$p(X_k, h_k|I_{1:k-1}) \sum \int p(X_k, h_k|X_{k-1}, h_{k-1}) p(X_{k-1}, h_{k-1}|I_{1:k-1}) dX_{k-1} \tag{12}$$

$$p(X_k, h_k|I_{1:k}) \propto p(I_k|X_k, h_k) p(X_k, h_k|I_{1:k-1}) \tag{13}$$

Given the previous object states and association hypotheses at frame $k-1$, the first equation predicts the states one step forward. The operation of this stage can be seen more clearly if we further factor the motion density:

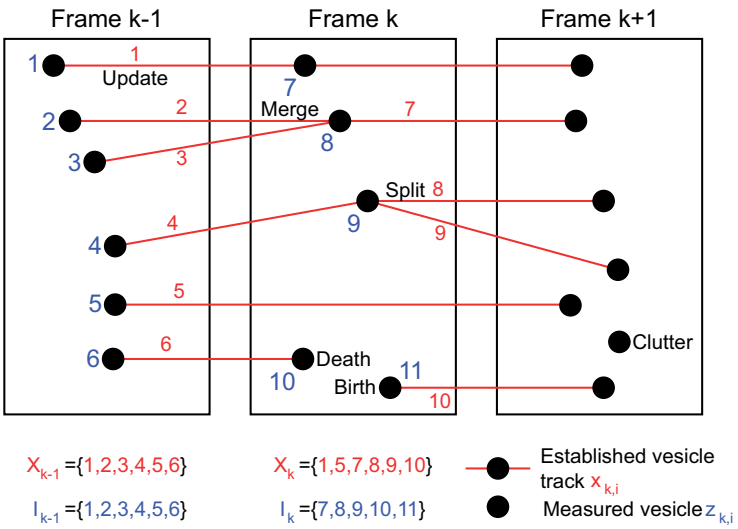

Figure 4: Vesicle tracking. An illustration of vesicle tracking over time. Several events can occur that change the number of tracks, such as merges and splits or birth and death of a vesicle track. Numbers in red indicate vesicle tracks, while numbers in blue represent the measured vesicles in each frame.

$$p(X_k, h_k | X_{k-1}, h_{k-1}) = p(X_k | h_k, X_{k-1}, h_{k-1}) p(h_k | X_{k-1}, h_{k-1}) \tag{14}$$

As shown the conditional state transition $p(X_k | h_k, X_{k-1}, h_{k-1})$ is following the evolution of the hypothesis $p(h_k | X_{k-1}, h_{k-1})$. Based on the reasoning of the motion model (Eq. (8)) and random measurements in the previous section, the hypothesis h_k helps to partition the objects and measurements into the different sets (Table 1). With this partitioning, each object track evolves independently, leading to the following joint probability density

$$p(X_k, h_k | X_{k-1}, h_{k-1}) = \prod_{\mathbf{x}_{k-1,i} \in \Phi} p_s(\mathbf{x}_{k-1,i})\, p(\mathbf{x}_{k,i} | \mathbf{x}_{k-1,i}) \prod_{\mathbf{x}_{k,i} \in B} p_b(\mathbf{x}_{k,i}) \tag{15}$$

where $\Phi = S_1 \cup S_2 \cup \Gamma \cup \Psi \cup D$, p_s is the probability that the object track will survive and p_b is the probability density of a new born object. Similarly, the measurements, conditioned on h_k, are statistically independent. Further assuming a state independent clutter model, the likelihood function (measurement density) can be obtained by:

$$\begin{aligned} p(I_k | X_k, h_k) = & \prod_{\mathrm{x}_{k|k-1,i} \in S_1} p_d(\mathrm{x}_{k|k-1,i})\, p(\mathrm{z}_{k,m} | \mathrm{x}_{k|k-1,i}) \\ & \times \prod_{\mathrm{x}_{k|k-1,i} \in S_2} \left(1 - p_d(\mathrm{x}_{k|k-1,i})\right) \prod_{\mathrm{x}_{k|k-1,i} \in \Psi} p_\Psi(\mathrm{x}_{k|k-1,i}) \\ & \times \prod_{\binom{\mathrm{x}_{k|k-1,i}}{\mathrm{x}_{k|k-1,j}} \in \Gamma} p_\Gamma(\mathrm{x}_{k|k-1,i}, \mathrm{x}_{k|k-1,j}) \prod_{\mathrm{z}_{k,i} \in C} p_C \end{aligned} \tag{16}$$

where $p_d(\mathbf{x}_{k,i})$ is the state dependent probability of detection, $p_\Gamma(\mathbf{x}_{k,i}, \mathbf{x}_{k,j})$ is the object tracks merge density, $p_\Psi = (\mathbf{x}_{k,i})$ is the object track split density, and p_C is the clutter density. As in Eq. (13), the likelihood is used to modify the predicted states $p(X_k, h_k | X_{k-1}, h_{k-1})$.

Table 1: Vesicle track hypothesis. Each hypothesis is a measurement-to-track association, which defines a set of compatible vesicle tracks.

	Object in frame $k-1$	Prediction $k \mid k-1$	Object in frame k	Measurement in frame k	Hypothesis h_k
S_1 (update)	$\mathbf{x}_{k-1,i}$	$\mathbf{x}_{k\|k-1,i}$	$\mathbf{x}_{k,i}$	$\mathbf{z}_{k,m}$	Object $\mathbf{x}_{k-1,i}$ is associated with exactly one measurement
S_2 (update)	$\mathbf{x}_{k-1,i}$	$\mathbf{x}_{k\|k-1,i}$	$\mathbf{x}_{k,i}$	ϕ	Object $\mathbf{x}_{k-1,i}$ does not associate with any measurement
Γ (merge)	$\binom{\mathbf{x}_{k-1,i}}{\mathbf{x}_{k-1,j}}$	$\binom{\mathbf{x}_{k\|k-1,i}}{\mathbf{x}_{k\|k-1,j}}$	$\mathbf{x}_{k,m}$	$\mathbf{z}_{k,m}$	If two objects $\mathbf{x}_{k-1,i}$ and $\mathbf{x}_{k-1,j}$are associated with the same measurement $\mathbf{z}_{k,m}$, they merge into a new object $\mathbf{x}_{k,m}$
Ψ (split)	$\mathbf{x}_{k-1,i}$	$\mathbf{x}_{k\|k-1,i}$	$\binom{\mathbf{x}_{k,m}}{\mathbf{x}_{k,n}}$	$\binom{\mathbf{z}_{k,m}}{\mathbf{z}_{k,n}}$	If object $\mathbf{x}_{k-1,i}$ is associated with two different measurements $\mathbf{z}_{k,m}$and $\mathbf{z}_{k,n}$, it may split into two objects $\mathbf{x}_{k,m}$ and $\mathbf{x}_{k,n}$
B (birth)	ϕ	ϕ	$\mathbf{x}_{k,i}$	$\mathbf{z}_{k,i}$	If measurement $\mathbf{z}_{k,i}$ is not associated with an existing object, it may represent a born object
D (death)	$\mathbf{x}_{k-1,i}$	$\mathbf{x}_{k\|k-1,i}$	ϕ	ϕ	Object $\mathbf{x}_{k-1,i}$ does not associate with any measurement
C (clutter)	ϕ	ϕ	ϕ	$\mathbf{z}_{k,i}$	If measurement $\mathbf{z}_{k,i}$ is not associated with an existing object, it may represent a clutter
Unions	X_{k-1}	$X_{k\|k-1,i}$	X_k	Z_k	

Next, we look at the model's ingredients. The transition density $p(\mathbf{x}_{k,i}, \mathbf{x}_{k,j})$ in Eq. (15) expresses a single object motion model, which is object type dependent corresponding to different motion patterns. Currently we use a first order discrete time linear statistics model (Bar-Shalom and Li, 1993):

$$x_k = F_k \mathbf{x}_{k-1} + \mathbf{v}_k \tag{17}$$

to describe the vesicle's position and velocity, where F_k is the state transition matrix defining the deterministic component of the model and $\mathbf{v}_k$ is a multivariate Gaussian random variable. Note that the vesicle index i has been omitted for simplification. Adopting this general model partially reflects our lack of knowledge about the dynamics of cell constituents, but exchange of the model into other forms is straightforward.

The likelihood function $p\left(\mathbf{z}_{k,m}\middle|\mathbf{x}_{k|k-1,i}\right)$ for individual objects in Eq. (16) incorporates both location and appearance information of the object. For simplicity we omit the time index, the measurement likelihood is defined as:

$$p(\mathbf{z}_m|\mathbf{x}_i) \propto \exp\left\{-\frac{(z_m - x_i)^2}{\sigma_d^2}\right\} \exp\left\{-\frac{(1-\rho[A_i, A_m^*])}{\sigma_A^2}\right\} \tag{18}$$

where the first term is the distance part, x_i is the object's predicted position (using Eq. (17)) and z_m the measured position, σ_d accounts for the measurement noise. However, considering that an object may suddenly change its motion and that the dynamic model is only an approximation of the vesicle's dynamics, the distance measure along can be inadequate. It is therefore introduced into the likelihood the second term: a measure of the similarity between the known vesicle in track i and measurement m. A_i and A_m^* are appearance model as defined by Eq. (5), σ_A is the noise term and ρ is the Bhattacharyya distance (Kailath, 1967) which measures the similarity of two discrete probability distributions.

$$\rho[A_i, A_m^*] = \sum \sqrt{p_u p_u^*} \tag{19}$$

The larger ρ is the more similar between A_i and A_m^*.

The vesicle split density $p_\Psi\left(\mathbf{x}_{k|k-1,i}\right)$ in Eq. (16) appears hard to define. We use the following equation:

$$p_\Psi(\mathbf{x}_i) = L(\mathbf{x}_i, \mathbf{z}_m) L(\mathbf{x}_i, \mathbf{z}_n) p_{sim}(A_m^*, A_n^*) \tag{20}$$

Where $L(\mathbf{x}_i, \mathbf{z}_m) = p_d(\mathbf{x}_i) p_d(\mathbf{z}_m|\mathbf{x}_i)$ is the likelihood that the measurement $\mathbf{z}_m$ comes from the object track $\mathbf{x}_i$,similarly for $L(\mathbf{x}_i, \mathbf{z}_n)$. p_{sim} expresses the criteria about the object track split, which is application and/or experimental dependent. Currently an object i is considered to have split into two objects m and n if the appearance A_m^* of m and the appearance A_n^* of n are similar.

Similarly, the object merge density is defined as

$$p_\Gamma\left(\mathbf{x}_i, \mathbf{x}_j\right) = L(\mathbf{x}_i, \mathbf{z}_m) L\left(\mathbf{x}_j, \mathbf{z}_m\right) p_{mer} \tag{21}$$

Where p_{mer} is the weighting factor dependent on the criteria about the object track merge, currently we set this factor to 1.

3.4 An efficient implementation

We have presented a method capable of tracking a variable number of vesicles in an optimal way, but for formation and maintenance of hypothesis the computational complexity increases rapidly with the number of objects. A sample scenario is shown in Figure 5. It is clear that to enumerate and keep all the hypotheses propagating over time would be infeasible. It is also shown how to resolve the problem of matching received measurements with established vesicle tracks is critical, because at each new frame, the new hypotheses are generated using the detected vesicles and the existing tracks.

A proposed method in the literature for optimal asymmetric assignment is the auction algorithm (Bertsekas, 1989). Under its framework, the association problem (Eq. (11)) is formulated as

$$\arg\max_{h} \sum_{n} \sum_{m} L(n,m)\, h(n,m) \tag{22}$$

where $m \in \{0\} \cup \mathcal{M}_k$ and $n \in \{0\} \cup \mathcal{T}_{k-1}$ are used to index the measurement set and the track set, $m = 0$ indicates a missed detection, and $n = 0$ represents a new source which could either be a new object track or a clutter. $h(n,m)$ is an assignment indicator defined as

$$h(n,m) = \begin{cases} 1 & \text{if measurement } m \text{ is assigned to track } n \\ 0 & \text{otherwise} \end{cases} \tag{23}$$

$L(n,m)$is the assignment weight, i.e. the likelihood of matching measurement m with vesicle track n. Based on the discussion in the previous section, it is given by

$$L(n,m) = \begin{cases} p_d p(\mathrm{z}_m|\mathrm{x}_n) & m > 0, n > 0 \\ p_{new} & m > 0, n = 0 \\ 1 - p_d & m = 0, n > 0 \end{cases} \tag{24}$$

where p_d is the probability of detecting a vesicle, $p(\mathbf{z}_m|\mathbf{x}_n)$ is the measurement likelihood defined in Eq. (18). p_{new} is experiment specific and dependent on density new of clutter p_C and new born object p_b. In our current implementation, p_d and p_{new} are set to fixed values, but substitution into other expressions is straightforward.

The auction algorithm solves Eq. (22) iteratively based on a one-to-one assignment, except for $m = 0$ or $n = 0$ which are allowed multiple assignments:

$$\sum_{n \in 0 \cup \mathcal{T}_{k-1}} h(n,m) = 1 \ \text{ for } m \in \mathcal{M}_k \tag{25}$$

Constrains that each measurement can have only one source, and

$$\sum_{m \in 0 \cup \mathcal{M}_k} h(n,m) = 1 \ \text{ for } n \in \mathcal{T}_{k-1} \tag{26}$$

constrains that each established track can associate with only one measurement. For our example scenario in Figure 5, the result of assignments made by the auction

algorithm is shown in Figure 6A. The auction algorithm has assigned the established vesicle tracks and measurements into one of the four sets: track set $\mathcal{T}^1$, in which each track is associated with exactly one measurement of the measurement set $\mathcal{M}^1$; track set $\mathcal{T}^0$ for tracks having no measurements assigned to it, and measurement set $\mathcal{M}^0$ for measurements not assigned to any existing tracks. In Figure 6A, $\mathcal{T}^1 = \{\mathbf{x}_{k-1,1}, \mathbf{x}_{k-1,3}, \mathbf{x}_{k-1,4}\}$, $\mathcal{M}^1 = \{\mathbf{z}_{k,1}, \mathbf{z}_{k,2}, \mathbf{z}_{k,3}\}$, $\mathcal{T}^0 = \{\mathbf{x}_{k-1,2}\}$ and $\mathcal{M}^0 = \{\mathbf{z}_{k,4}\}$. The one-to-one auction algorithm appears inadequate for our problem. As discussed in the previous section, there are cases where two tracks may be associated with one measurement, e.g., when two vesicles are crossing, they may produce a single unresolved measurement; or when two vesicles merge, there will be only one measurement in the next frame. Similarly, one track may have two measurements assigned to it as a result of vesicle split. To compensate for "merged" and "split" measurements, we propose a second round assignment (Tsaknakis et al., 1991; Kirubarajan et al., 2001). The assignment is made between $\mathcal{T}^0$ and $\mathcal{M}^1$, $\mathcal{T}^1$ and $\mathcal{M}^0$ (Figure 6B).

Figure 6C shows seven tracks formed after two times application of the auction algorithm. Each track corresponds to a different data association hypothesis. For a track formed during $\mathcal{T}^1$ and $\mathcal{M}^0$ assignment, its assignment weight (Eq. (24)) must be modified to reflect the split event (Eq. (20)). For example, the assignment weight for track 7 is changed to $p_d p(\mathbf{z}_{k,4}|\mathbf{x}_{k-1,4}) p_{sim}(A^*_{k,3}, A^*_{k,4})$.

The tracks formed at frame k are propagated to frame $k+1$ (Eq. (17)) and associated with measured objects through the two-round auction algorithm. In Figure 7A, nine tracks are formed. Because the tracks formed by branching in the second round auction assignment at time k can represent at most one vesicle track, they are alternatives and incompatible. For example, referring to Figure 7A, the tracks 2,3,8 are incompatible, the same goes for the track 6,7,9.

We rank each track using the sum of its assignment weights over two frames, and resolve the track clash by selecting the most likely hypothesis. In example of Figure 7A, this is accomplished by computing $(L_2 + L_4)$, $(L_3 + L_4)$ and $(L_8 + L_4)$, where L is the track assignment weight. Suppose $(L_8 + L_4)$ is the maximum of the three, L will be selected and the established vesicle track $\mathbf{x}_{k-1,2}$ will be associated with measurement $\mathbf{z}_{k,2}$. Similarly, by computing and comparing $(L_6 + L_5)$, $(L_7 + L_5)$ and $(L_9 + L_5)$, the most likely hypothesis is chosen as to match measurement $\mathbf{z}_{k,4}$ with vesicle track $\mathbf{x}_{k-1,4}$. The assignments after hypothesis selection are shown in Figure 7B. These assignments will be used to update established tracks forward (Eq. (13)) and assignment/selection process is repeated through the whole image sequence.

If two established vesicle tracks share the same measurements for three consecutive frames, they will be considered as merged into a new single vesicle. Any measurement that is not assigned to an existing track will be used to initiate a new track, but any track will not be confirmed until it lasts for at least three frames. This condition is necessary to exclude false detection in noisy images. If a track does not have a measurement assigned to it for three consecutive frames, it will be consider dead.

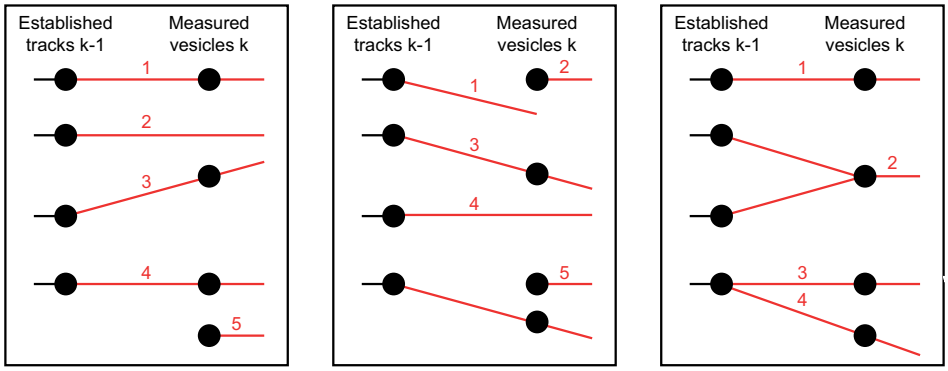

Figure 5: Multiple Hypothesis Tracking. An example of vesicle track hypothesis options. Vesicles along an established track can be linked to measured vesicles in the next frame in several different ways. The three different hypotheses lead to a different number of tracks.

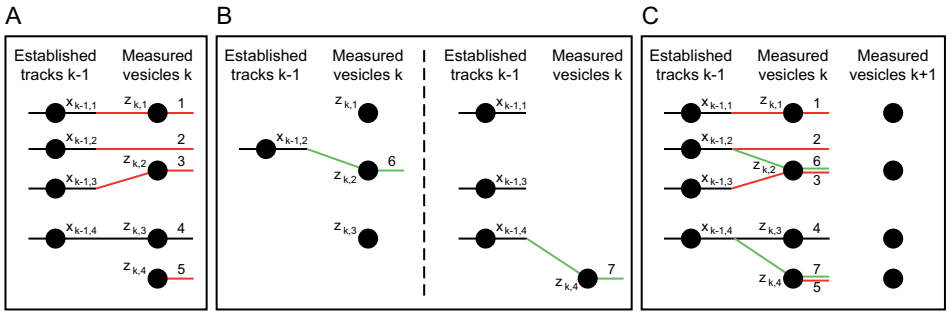

Figure 6: Multi-assignment. Illustration of the multi-assignment by the auction algorithm. (a) First round assignment. (b) Second round assignment. Left: the assignment between and ; Right: the assignment between and . (c) Tracks formed through multi-assignment auction algorithm contain incompatible hypotheses, but the evaluation of hypotheses will use information in the next frame.

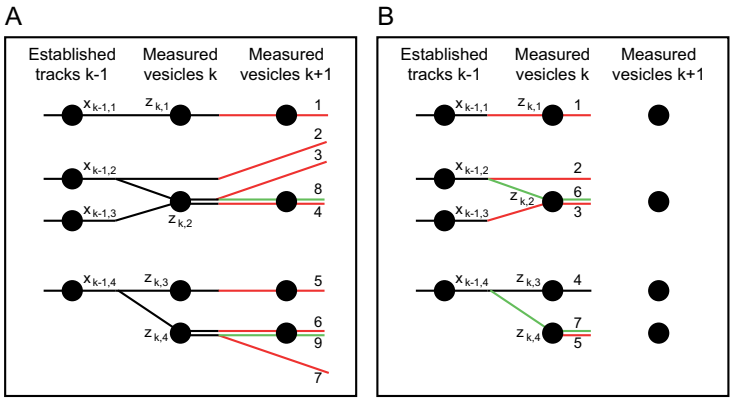

Figure 7: Hypothesis maintenance. Example of hypothesis maintenance. (a) The hypothesis is selected based on the auction algorithm assignments over two consecutive frames, which allows evaluation to be performed on a more global level while avoids to keep track of a very large number of hypotheses. (b) Track update is based on the selected most likely hypothesis.

REFERENCES

Bar-Shalom, Y., and Li, X.-R. (1993). Estimation and tracking: principles, techniques and software (Norwood, MA: Artech House, Inc)

Bertsekas, D. P. (1989). The auction algorithm for assignment and other network flow problems. Interfaces, 133-149.

Blackman, S., and Popoli, R. (1999). Design and analysis of modern tracking systems (Norwood, MA: Artech House)

Cheng, Y. (1995). Mean shift, mode seeking, and clustering. IEEE Trans Pattern Anal Mach Intell *17*, 790-799.

Clark, D., Panta, K., and Vo, B. (2006). The GM-PHD filter multi-target tracker. In Proc. 8th International Conference on Information Fusion.

Comaniciu, D., Ramesh, V., and Meer, P. (2003). Kernel-based object tracking. IEEE Trans Pattern Anal Mach Intell, 564-577.

Comaniciu, D., Ramesh, V., and Meer, P. (2000). Real-time tracking of non-rigid objects using mean shift. In Proc IEEE Conf Comp Vis Patt Recogn 2000.

Gonzalez, J., Rojas, H., Ortega, J., and Prieto, A. (2002). A new clustering technique for function approximation. IEEE Trans neural netw *13*, 132-142.

Kailath, T. (1967). The divergence and Bhattacharyya distance measures in signal selection. IEEE Trans Commun Techn *15*, 52-60.

Kirubarajan, T., Bar-Shalom, Y., and Pattipati, K. R. (2001). Multiassignment for tracking a large number of overlapping objects [and application to fibroblast cells]. IEEE Trans Aerosp and Electron Syst *37*, 2-21.

Ku, T.-C., Huang, Y.-N., Huang, C.-C., Yang, D.-M., Kao, L.-S., Chiu, T.-Y., Hsieh, C.-F., Wu, P.-Y., Tsai, Y.-S., and Lin, C.-C. (2007). An automated tracking system to measure the dynamic properties of vesicles in living cells. Microsc Res Tech *70*, 119-134.

Mahler, R. P. S. (2003). Multitarget Bayes filtering via first-order multitarget moments. IEEE Trans Aerosp and Electron Syst *39*, 1152- 1178.

Mahler, R. P. S. (2002). A theoretical foundation for the Stein-Winter "probability hypothesis density (PHD)" multitarget tracking approach. MSS Nat'l Symp. on Sensor and Data Fusion.

Otsu, N. (1979). A threshold selection method from gray-level histograms. IEEE Trans Syst Man Cybern *9*, 62-66.

Reid, D. (1979). An algorithm for tracking multiple targets. IEEE trans autom contr *24*, 843-854.

Sezgin, M., and Sankur, B. (2004). Survey over image thresholding techniques and quantitative performance evaluation. J electron imaging *13*, 146-168.

Shalom, Y. B., and Fortmann, T. E. (1988). Tracking and data association (Boston: Academic-Press).

Tsaknakis, H., Buckley, M. D., and Washburn, R. B. (1991). Tracking closely-spaced objects using multi-assignment algorithms. Tri-Service Data Fusion Symposium.

Vo, B.-N., Singh, S., and Doucet, A. (2005). Sequential Monte Carlo methods for multitarget filtering with random finite sets. IEEE Trans Aerosp and Electron Syst *41*, 1224- 1245.

APPENDIX B

NEDERLANDSE SAMENVATTING

DYNAMIEK VAN DE GROEI CONUS EN BLAASJES TRANSPORT IN GEKWEEKTE NEURONEN TIJDENS DE ONTWIKKELING.

Samenvatting

De ontwikkeling van de hersenen van gewervelden zoals de mens doorloopt verschillende stadia, waarbij cellen zich vermenigvuldigen, specialiseren en aanpassen aan hun omgeving. Cellen beginnen met delen waarna een gedeelte zich specialiseren in bijvoorbeeld zenuwcellen, terwijl andere cellen zich specialiseren tot astrocyten en ondersteuning bieden voor de zenuwcellen. Tijdens de ontwikkeling van de hersenen doorlopen dehersencellen verschillende stadia. Deze stadia zijn nauwkeurig bestudeerd door cellen uit embryonaal weefsel te isoleren en te kweken. Hieruit bleek dat de hersencellen 5 specifieke stadia doorlopen: eerst ontstaan er plooien in het membraan. Deze plooien worden lamellopodia genoemd. In het volgende stadium groeien verschillende processen vanuit het cellichaam (de neurieten).

Zenuwcellen hebben een speciale compartimentalisatie: een zenuwcel heeft meerdere neurieten die opgedeeld kunnen worden in twee groepen: neurieten die signalen ontvangen (de dendrieten) en een neuriet die signalen verzend (het axon). Een zenuwcel heeft meerdere dendrieten, maar slechts een axon. Tijdens het volgende stadium zal het axon snel uitgroeien op zoek naar andere zenuwcellen. Dit uigroeien wordt gereguleerd door verschillende sensoren op het oppervlak van een speciaal compartiment aan het uiteinde van het axon (de groei-conus). Dit handvormige compartiment tast de omgeving af op zoek naar signalen die aangeven welke kant het axon op moet.

Nadat het axon uitgegroeid is, gaan de dendrieten uitgroeien. De dendrieten leggen veel kortere afstanden af maar zijn vaak meer vertakt vergeleken met het axon. Het volgende en laatste stadium van de ontwikkeling is het vromen van contacten tussen axonen en dendrieten, de zogenaamde synapsen. Dit zijn de punten waarop signalen van de ene zenuwcel overgedragen worden aan de volgende zenuwcel enzovoort. Deze synapsen zijn belangrijk voor het functioneren van de hersenen en spelen een belangrijke rol in het verwerken van informatie en leren en geheugen. Synapsen worden gevormd door twee compartimenten die gescheiden worden door een kleine ruimte. Aan de ene zijde is de presynaps, die zich bevindt op het axon, en aan de andere kant zit de postsynapsop de dendriet. Signaaloverdracht vindt plaats doordat speciale blaasjes (synaptische vesicles) fuseren met de presynaptische membraan en hun lading van signaalstoffen (neurotransmitter) afgeven als de presynaps een elektrische puls ontvangt. Deze signaalstoffen binden aan receptoren op de postsynaptische membraan en wekken daar een elektrische puls op. Deze puls gaat naar het cellichaam en kan dan doorgegeven worden via het axon naar de volgende cel.

Naast de synaptische vesicles bestaat er nog een tweede groep blaasjes die kunnen fuseren met het membraan en stoffen uitscheiden. Deze blaasjes bevatten kleine

eiwitten in een compacte matrix en laten onder een electronenmicroscoop een donkere kern zien en worden daarom dense core vesicles genoemd. Deze blaasjes zijn belangrijk voor de vorming van synapsen: de eiwitten die ze bevatten stimuleren het vormen van de synaptische elementen (pre- en postsynaps). Verder spelen ze ook een rol in het stabiliseren van de synaptische contacten.

In dit proefschrift wordt de rol van deze twee type blaasjes bekeken op de ontwikkeling van de zenuwcellen. Met behulp van speciale muizen die specifieke genen missen die essentieel zijn voor het fuseren van synaptische blaasjes met de membraan, is het mogelijk om de rol van deze blaasjes in de beginstadia van de ontwikkeling van dezenuwcel te ontrafelen. Door de eiwitten die zich in de dense core vesicles bevinden te voorzien van een fluorescent label kan de dynamiek van deze blaasjes bestudeerd worden: zowel het transport door de neurieten als het fuseren met de membraan. Verder wordt hier ook nog een techniek beschreven om dit transport op een geautomatiseerde wijze te analyseren. Ook worden twee technieken beschreven die helpen om het proces van fuseren van blaasjes met het membraan te bestuderen. De ene techniek staat het toe om het fuseren van blaasjes te observeren zonder het toepassen van fluorescente labels. De andere techniek staat het toe om de benodigdheden voor vesicle fusie met behulp van licht nauwkeurig te manipuleren.